Analytical Cellular Pathology 35 (2012) 145–163
DOI 10.3233/ACP-2011-0048
IOS Press

Review Article: Modern Trends in Imaging VI

Raman scattering in pathology

Zachary J. Smith[a], Thomas R. Huser[a,b] and Sebastian Wachsmann-Hogiu[a,c,*]
[a]*Center for Biophotonic Science and Technology, University of California, Davis, CA, USA*
[b]*Department of Internal Medicine, University of California, Davis, CA, USA*
[c]*Department of Pathology, University of California, Davis, CA, USA*

Abstract. Raman scattering is the inelastic scattering of light by chemical bonds, and can therefore show molecular specificity. It can be used both in pure spectroscopy mode, and in imaging mode. While many applications of Raman spectroscopy and imaging in the biomedical field have been so far demonstrated, the use of this technology for pathology applications is still in its early stages. In this paper we review some of the most important recent developments in this field, including a description of relevant technologies, applications to molecular sensing, characterization of cells and tissues of interest, and disease detection via Raman scattering.

Keywords: Raman scattering, imaging, molecular sensing, diagnosis

1. Introduction

Raman scattering occurs by the inelastic scattering of photons by molecular bonds. In this scattering event a small fraction of the incident photons exchange energy with the molecular vibration and are scattered. The scattered photons can either be red-shifted by providing energy to the bond vibration ("Stokes" Raman scattering) or blue-shifted by receiving energy from the bond ("anti-Stokes" Raman scattering), with the difference in energy between the incident and scattered photons corresponding to the energy of the molecular vibration. Detection of these scattered photons yields a spectrum containing several Raman peaks, each of which being characteristic of a specific molecular bond. Collectively, these peaks provide an intrinsic "molecular fingerprint" of the sample (the Raman spectrum), resulting in a wealth of information about the chemical bonds associated with various molecules present in tissues and cells. This information can be used in different biomedical applications, such as (i) analysis of chemical composition (DNS, RNA, lipids, proteins, etc.) and presence of certain molecular markers (sensors and assays), (ii) study of the interactions between macromolecules (DNA-protein, protein-lipid interactions), (iii) monitoring biological functions (lipid uptake, enzymatic activity, neurological function, mapping of intracellular chemical environment), (iv) diagnosis and characterization of disease (cancer, atherosclerotic plaques), or (v) label free microscopy and endoscopy [1].

While chemical specificity without the use of labels, noninvasiveness, and the very good spatial resolution are the main advantages of Raman scattering based techniques, there are significant drawbacks related to the weak signal, the usually much stronger fluorescence background, and the limited penetration depth typical for optical techniques. Several Raman-based techniques have been developed to address these limitations and perform measurements in different situations in which biomedical samples can be found.

Spontaneous Raman spectroscopy is mostly used in the near-infrared region where laser damage and excitation of autofluorescence is minimal and light

*Corresponding author: S. Wachsmann-Hogiu, Center for Biophotonic Science and Technology, University of California, CA, Davis, USA. E-mail: sebastian.wachsmann@cbst.ucdavis.edu.

penetrates deeper into tissue. This technique is very suitable for applications such as monitoring changes in cellular composition as a function of malignancy, or classification of cells and bacteria. The signal obtained in these situations is, however, very weak, and several techniques have been developed to increase the intensity of the Raman scattering signal.

One way is to choose the excitation wavelength within the electronic resonance (absorption band) of a certain molecule. In this case the process is called Resonance Raman Scattering (RRS) and the Raman signal will increase by up to 5 orders of magnitude. However, it is usually associated with a much stronger fluorescence background, and additional approaches such as ultrafast optical switches, background subtraction, spatially offset Raman scattering, or multi-excitation are needed for the rejection of this background. Among these techniques, time-gated Raman spectroscopy at high repetition rates and low energy per pulse has great promise, as it may allow the detection of resonance Raman signals of biological specimens [2].

Other techniques such as Coherent Anti-Stokes Raman Scattering (CARS) and Stimulated Raman Scattering (SRS) allow for additional coherent amplification of the Raman signal and can be used either in resonance or out of resonance with the electronic states of the molecule. The CARS signal is generated when two lasers are focused into the sample, one acting as the source leading to Stokes-shifted Raman scattering, while the other one is tuned to the same frequency as a specific Raman peak [3, 4]. The two lasers interact nonlinearly within their overlap volume, simultaneously exciting the characteristic chemical vibration, and driving the amplification of the corresponding anti-Stokes peak. The resulting CARS signal is more than a thousand times stronger than the original Raman signal and can be used for chemically selective imaging without the use of fluorescent tags or dyes. By significantly reducing the exposure time required to record the signal, CARS holds great promise for imaging living cells and tissues. The SRS signal is generated by the coherent interaction of a pump and a Stokes beam, whereas the difference between their frequencies matching the frequency of a Raman vibration. As a result of coherent excitation of molecular vibrations, the intensity of the pump beam decreases and that of the Stokes beam increases. While these changes are very small compared with the initial laser intensities, high-frequency modulation techniques are needed to record a useful signal [5, 6]. Due to the lack of a non-resonant background (which typically plagues CARS), this techniques claims great promise for video-rate *in vivo* label free molecular imaging.

Surface Enhanced Raman Scattering (SERS) is another way to amplify the Raman signal by the presence of metallic nanoparticles that exhibit plasmon resonance. In SERS, molecules adsorbed onto the surface of these nanoparticles show strong Raman enhancement, up to 15 orders of magnitude, due to the generation of an enhanced electric field around the particle and charge transfer mechanism. The nanoparticles must be on the order of tens of nanometers in diameter to exhibit plasmon resonance, and the excitation wavelength has to be within this plasmon resonance in order to achieve enhancement. Aggregation of the nanoparticles, as well as their shape can shift the position of the plasmon resonance. Due to extremely large enhancement factors, Raman spectra of single molecules can be detected, which makes this technique attractive for biosensing. Additionally, SERS can yield molecular structural information, has the potential to be broadly multiplexed, and has the unique ability to improve the specificity of detection by distinguishing between specific and non-specific binding events [7]. Molecular beacon assays measuring combined fluorescence and SERS signals of a reporter molecule were developed for the detection of human viral RNA [8], while an aptamer-based SERS sensor using methylene blue as a Raman probe was developed for thrombin detection [9]. Folic acid in water and human serum was detected in this way by using silver nanoparticles created via ethylene-diaminetetraacetic acid reduction [10]. It was also shown that very low concentrations of melamine in food could be detected using commercially available SERS-active substrates [11]. The prospect of label-free DNA detection in high-density arrays is discussed in [12] by using a SERS platform based on island film lithography combined with silver deposition by galvanic exchange. By using small, specific oligonucleotide sequences, Pal et al. developed a SERS gene probe for breast cancer [13].

In this article we will highlight applications of various Raman techniques to problems in pathology ranging in scale from the *in vitro* analysis of single cells to the *in vivo* spectroscopy and imaging of tissues and entire organisms. Figure 1 briefly summarizes typical spectra that can be obtained with Raman spectroscopy on various tissue components, ranging from bacteria and cells to skin and bone.

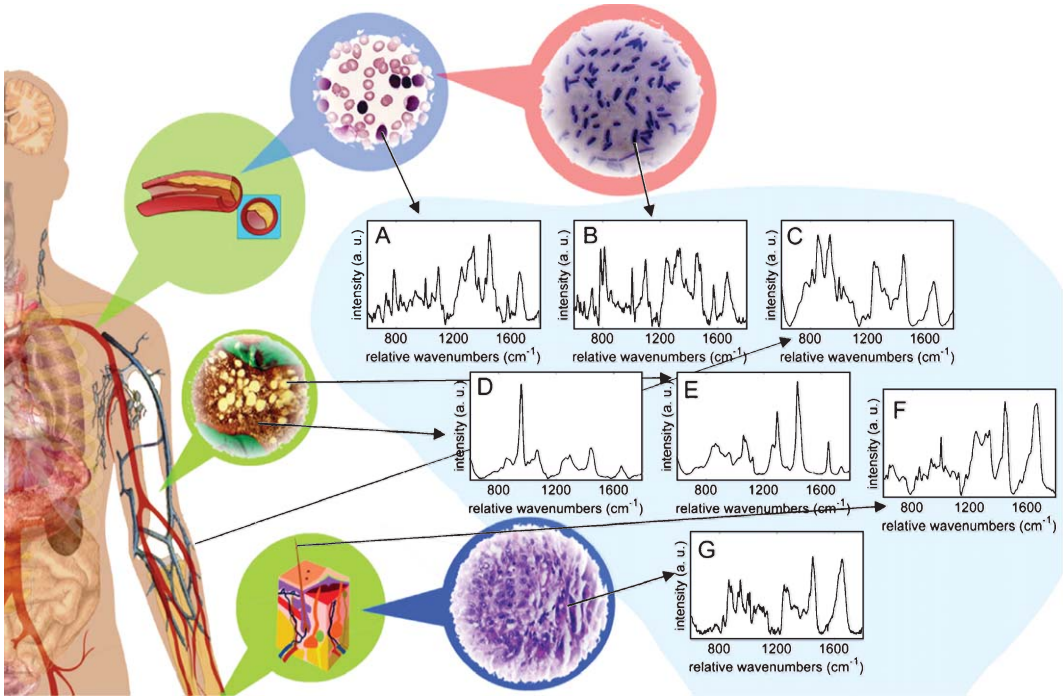

Fig. 1. Typical Raman spectra of various tissue components. A) T-cell; B) streptococcus pneumoniae; C) bovine tendon; D) porcine bone matrix; E) porcine yellow marrow; F) gray human hair; G) human skin epithelial tissue. All spectra were measured with a home-built Raman spectrometer with excitation at 785 nm.

2. Data processing methods in vibrational spectroscopy

Obtaining high quality results from home-built (and commercial) Raman systems is not always a trivial matter, as Raman spectra may be contaminated by fluorescence backgrounds, or may have been collected with low signal-to-noise in order to minimize exposure times (especially for imaging or clinical applications). Furthermore, Raman spectra from biological samples are typically composed of multiple overlapping peaks due to the chemically rich nature of biological tissues. Therefore assessing differences in spectra from different samples or different regions within a sample may necessitate the use of data processing and analysis techniques that may not be familiar to a non-spectroscopist.

The signal challenge in most spontaneous Raman spectroscopy applications is background correction, which must be done in a consistent and appropriate way to ensure that spectral differences are real and not artifact. A common technique is to model the background as a slowly varying function that can be well approximated by a low-order polynomial, which is then subtracted from the spectrum. Various schemes to estimate the polynomial function exist, with by far the most common being the modified polyfit method devised by Lieber and Mahadevan-Jansen [14]. This method works well for featureless backgrounds, but can fail in cases where a spectral contaminant is sharply featured. An extension to the modified polyfit to account for known (sharply featured) spectral contaminants was developed by Beier and Berger [15]. Other, more complex methods also exist, such as shifted-excitation-difference Raman spectroscopy (SERDS) and the related Modulated Raman Scattering technique [16, 17]. Both techniques aim to eliminate the background by means of slightly changing the excitation wavelength between two or more sequential acquisitions. Because the Raman peaks will shift along with the excitation wavelength while the background will largely stay fixed, finding the difference between the sequential frames will yield a derivative of the original, background free spectrum.

After corrected spectra are obtained, one is typically left with a large dataset consisting of several tens to hundreds of spectra, each spectrum typically hun-

dreds to thousands of wavenumbers long. In order to efficiently reduce this data to only the most valuable information, a technique known as Principal Components Analysis (PCA) is used. Although a thorough treatment of PCA would involve a detailed discussion using linear algebra, the technique can be concisely summarized in the following way. Consider a complicated spectrum consisting of many different peaks. For different samples these peaks' intensities and positions may shift, corresponding to chemical differences between the samples. However, each peak is not likely to move independently, as each individual chemical within the system is represented by multiple peaks, and multiple chemicals are often varying in tandem. Principal Components Analysis seeks to tease out which pixels vary together, and how much does their variation explain the variation of the dataset as a whole. PCA composes a new linear model of the spectral dataset where each spectrum is represented by different concentrations of Principal Components, where the first component are those grouped variations that explain the most variance in the dataset. After that component is removed, the second Principal Component describes the most variation of what is left, and so on. In most well designed experiments, one would expect the variation between groups of interest to be one of the dominant sources of variance. Therefore, PCA is a sensible technique to discover those differences. In this way, a spectrum formerly composed of thousands of datapoints can be reduced to two or three principal component concentration values (or scores) that are sufficient to describe all of the relevant data contained within that spectrum. Plotting each spectrum in a two or three dimensional space defined by the principal component scores can then allow very intuitive visualization of the differences between groups, as shown in Fig. 2, adapted from Ref. [18]. PCA belongs to a class of techniques that can be grouped under the heading of multivariate data reduction methods that all have as their goal the distillation of a spectrum into a few numbers that succinctly describe its chemical information.

Often what is desired in a spectroscopy application is not any detailed information about chemical or spectral content, but rather to assign a sample into one of several groups (healthy vs. diseased, bacterial type or strain, etc.). Often the differences between these groups may be subtle and not always amenable to a crude visual analysis. In such cases the spectra (or their relevant principal component scores) are submitted to a

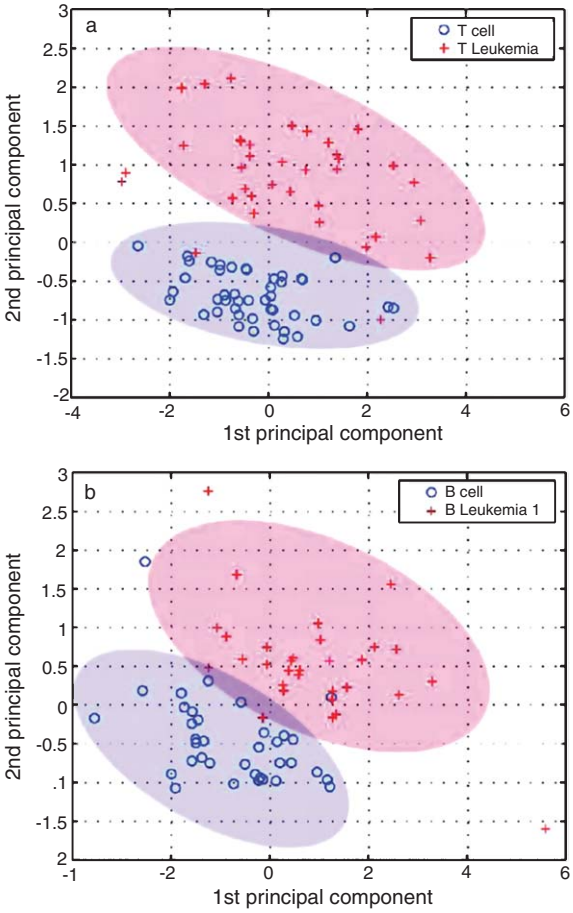

Fig. 2. Principal component scatter plots comparing normal and leukemic (a) T cells and (b) B cells. Adapted with permission from Ref. 18.

classification algorithm. Several are common, including logistic regression [19], neural networks [20], and support vector machines [21], to name a few. All take spectra or scores as inputs, and then through various linear and nonlinear data transformations attempt to create diagnostic functions that exaggerate between group differences while minimizing within group differences. A training set, where group member status is known for each spectrum, is used to derive the diagnostic functions. Following training, validation sets may be used to evaluate performance and ensure that robust and reproducible results are obtained, as well as to quantify the expected classification errors. Each spectrum in the validation set is placed within one of several *a priori* defined groups, occasionally with Bayesian probabilities attached to the confidence with which the spectrum was classified. Utilizing these

"supervised" techniques can provide quantitative estimations of group membership based on chemical content as reported by the Raman spectrum.

A related class of classification techniques falls under the heading of "unsupervised" classifiers. These can be particularly valuable in imaging and other applications where *a priori* groups are unknown. A common unsupervised technique is called hierarchical cluster analysis (HCA). Cluster analysis represents each spectrum as a single point in a high dimensional space, where each axis represents one pixel on the spectrum, and the location along that axis represents the intensity of the spectrum at that pixel. Pairwise distances are calculated between each spectrum and each other spectrum within the dataset. Spectra whose pairwise distances indicate they are grouped together are assigned to one cluster, with the number of clusters being a user-selected variable. These techniques are valuable in imaging applications where there are hundreds or thousands of pixels that may all have fairly low signal-to-noise spectra associated with them (due to short integration times per pixel to keep the image acquisition times manageable). Using HCA, an image can be false colored based on the cluster a pixel is assigned to. The spectra of all pixels belonging to a single cluster can be averaged together to create a single "cluster" spectrum with correspondingly high signal to noise [22]. A second unsupervised technique is known as vertex component analysis (VCA). Understanding VCA requires us to introduce the concept of a simplex. A simplex is a geometric shape whose number of vertices is one greater than the dimension in which it resides. For example, in a 2-dimensional plane, a simplex would be a triangle (3 vertices). In a 3-dimensional volume, a simplex would be a pyramid (4 vertices). As in HCA, each spectrum is represented as a point in a high dimensional space. All of the spectra in a dataset can be thought of as occupying a geometric volume within that space. A simplex can be constructed such that it totally encloses the dataset while at the same time having a minimum total volume. The vertices of this simplex correspond to spectra, the "vertex component spectra". Each spectrum in the dataset can be constructed by mixing different concentrations of these vertex components. Again, in imaging, a pixel can be false-colored depending on the concentrations of each vertex component within that pixel. Although being perhaps conceptually more challenging than HCA, the assumptions underlying VCA are actually more reasonable. In HCA the assumption is that each pixel represents a spectrum of some pure class, and each spectrum is either representative of one class or another but in all cases is assumed to be 100% representative of that cluster. With VCA the assumption is that each spectrum is a linear superposition of several possible classes, with each spectrum sharing membership among several classes in varying proportions. This flexibility has led to increasing adoption of the VCA technique [23].

Raman spectra report on chemical content of samples, and as such can be exceedingly information-rich. However beneficial this information richness is, it can be a major challenge to extract the useful information from the wealth provided by the Raman spectrum. To accomplish this, many spectroscopists turn to multivariate data reduction and classification techniques such as those described above. Although these techniques (and others not described) have relative advantages, disadvantages, and caveats associated with them, they are essential for utilizing Raman spectra to their full advantage in answering biological and medical questions.

3. Raman spectroscopy for cellular analysis and imaging

Single cell Raman spectroscopy has gained dramatically in adoption since it was first demonstrated in the seminal paper by Puppels et al. published in the journal "Nature" in 1990 [24]. One of the main reasons why Raman spectroscopy has seen particularly explosive growth in the area of analysis, spectroscopy, and imaging of single cells can be explained by its unique strength in nondestructively analyzing the biochemical composition and metabolic states of cells without the need for exogenous probes, such as fluorescent molecules. Even more remarkable is that this analysis is achieved on length scales similar to those made accessible by confocal fluorescence microscopy [25].

3.1. Requirements for Raman cell analysis

Key to achieving the sensitivity to probe individual cells by Raman spectroscopy is the ability to reject background signals as effectively as possible. This has first been demonstrated by combining laser Raman spectroscopy with confocal microscope optics [26]. In confocal microscopy a laser beam is focused to a tight, diffraction-limited spot (∼250 nm diameter), which

is then magnified by the microscope optics and projected onto a confocal pinhole of 50–100 μm diameter. By requiring that the scattered light from the focused laser spot has to be funneled through this pinhole, any contributions or background signals from out-of-focus regions in the sample are automatically blocked by the pinhole and will not contribute to the signal spectrum. In more recent implementations the pinhole is often replaced by the core of a multimode optical fiber into which the Raman-scattered light is coupled. The fiber then delivers the scattered light to a grating spectrometer with an ultra-sensitive CCD camera for spectral data acquisition.

For practical reasons red to infrared laser light has proven to be most effective for obtaining single cell Raman spectra. This is mostly due to the fact that blue or green laser wavelengths lead to the excitation of substantial auto-fluorescence from the cells. It has also been shown that wavelengths below ~600 nm are typically harmful to cells [27] because they are significantly absorbed by various cellular components, such as proteins, amino acids, nucleic acids, or metabolites leading to either the photo-decomposition of these molecules or the generation of reactive oxygen species. Nonetheless, impressive examples of cellular imaging at wavelengths in the blue and green part of the optical spectrum have been demonstrated - however, typically on fixed cells. Implementations of cellular Raman spectroscopy can extend on length scales from zero dimensions (point mapping) to four-dimensional imaging where changes in local cellular states are monitored with time. In its simplest implementation, specific locations within a cell can be addressed either by manually selecting them with a micrometer-driven positioning stage or by point-by-point scanning and acquiring full Raman spectra for every spot location. A variation of this concept that can overcome background contributions has recently also gained popularity. In this case, the laser power used to induce Raman scattering is increased to the point where it can optically trap a cell by effectively functioning as a single beam optical tweezers [28–30]. Laser tweezers Raman spectroscopy (LTRS) as this concept has been termed, has the added benefit that cells can be analyzed several tens of microns away from any solid substrate, thus further reducing any background signals from such optical surfaces. Certain cellular buffer solutions, such as phosphate buffered saline (PBS) or Tris buffer have minimal to no Raman background while allowing us to keep cells in a somewhat arrested metabolic state. This enables the spectroscopic characterization of living non-adherent cells in their natural environment. Typically, LTRS utilizes mostly far-red to infrared lasers due to the aforementioned toxicity of lower laser wavelengths and the relatively high power levels required for optical trapping [29–31].

A more efficient way of acquiring Raman data across an entire cell is made possible by line scanning where a one-dimensional sample area (line) is illuminated and then imaged onto the entrance slit of an imaging spectrometer [32]. With a CCD camera of sufficient height (typically at least 400 lines vertically) as detector this allows for the simultaneous acquisition of Raman spectra from many sample points along the line. This concept is only limited by the laser power applied to the sample, the spatial resolution of the spectroscopy system, and potential crosstalk within the imaging spectrometer. By sweeping the line illumination across the sample image data can be acquired with significantly higher speed than with the point scanning technique. Lastly, Raman data can also be acquired by point scanning or wide-field illumination of the sample and imaging the sample through a narrow band-pass filter to isolate specific Raman resonances of interest [33]. By utilizing several such narrow filters or by utilizing a single filter with a tunable laser source, ratiometric Raman imaging is made possible, where spectral peaks of interest can be isolated and their behavior monitored with time. This mechanism, however, obviously doesn't allow for the acquisition of entire spectra for each pixel of the CCD chip. To make such an application possible, the band-pass filter would have to be tunable across a spectral range of interest. This can be achieved by utilizing electro- or acousto-optic tunable filters, or by angle-tuning of custom-made interference filters.

For completeness, we should note that over the last decade coherent Raman imaging methods have become increasingly popular for cellular imaging [3, 4, 34]. Here, a combination of pico- or femtosecond pulsed lasers is utilized to probe specific Raman resonances, e.g. those of lipid vibrations, very efficiently. One laser typically provides the pump beam that induces Raman scattering. The second laser beam is then tuned to a Raman resonance of interest (relative to the wavelength of the pump laser) and probes this Raman vibration by inducing stimulated emission of Raman-scattered photons which can either be detected directly by lock-in techniques (leading to stimulated Raman scattering, or SRS [35]) or which,

when combined with an additional pump photon leads to the emission of anti-Stokes Raman scattered photons (coherent anti-Stokes Raman scattering, CARS [3, 4]). Due to the use of short-pulsed lasers, this leads to the coherent probing of many Raman-active groups with the same vibrational mode simultaneously, and thus significantly stronger signals when compared to spontaneous Raman scattering with continuous-wave laser beams. By combining broadband femtosecond lasers with picosecond lasers, an entire region of the Raman spectrum can also be probed very efficiently. These techniques, however, require significant investments in laser infrastructure and, at least for now, the employment or consultation of experts in the operation of such lasers.

A particular problem with ultra-sensitive spontaneous Raman spectroscopy at the cellular level is that despite our best efforts in minimizing background contributions, adherent cells naturally have to grow on a substrate, which leads to Raman scattering in the substrate. While confocal microscope optics rejects much of this [36], it also typically requires the use of microscope objectives with high numerical aperture (NA). The most widely used choices are water immersion lenses (1.2 NA) or oil immersion lenses (1.4 NA). These, however require thin transparent substrates, such as glass coverslips with a nominal thickness between 150–220 μm, through which the sample is probed. Coverslips made from standard glass, such as BK7, are widely available but generate rather strong background signals from Raman scattering in the glass. This is acceptable if the cellular signals to be measured are equally strong, e.g. from intracellular lipid droplets. LTRS overcomes this problem by "lifting" and suspending the cells far enough above the substrate (~30 μm) while also requiring high NA optics. Fortunately, substrates with significantly lower intrinsic Raman scattering are available as well, e.g. coverslips made from fused silica (quartz), or magnesium fluoride (MgF_2) - albeit at very significant cost. Alternatively, metal mirrors or extended transparent substrates, i.e. CaF_2 can also be used, but require upright microscope designs and lower NA lenses.

In the first demonstration of single cell Raman spectroscopy, Puppels and coworkers utilized confocal optics to demonstrate that they could obtain Raman spectra from different locations within the same cell and that these spectra reflect the expected local cellular biochemistry (e.g. the nucleus exhibits contributions mostly from DNA and proteins, whereas the cytoplasm exhibits mostly protein signals, as well as contributions from metabolites, such as sugars [24]. They also demonstrated the ability to obtain spectra from isolated chromosomes. While, in the years to come, this research group was mostly isolated in its pursuit of single cell Raman spectroscopy, other researchers began to "see the light" in the mid to late 1990 s and soon a large number of Raman scattering studies at the cellular levels started to be published. These include the study of immune cells [37, 38] and their behavior upon encountering foreign objects, such as phagocytosis of antibody-coated beads by macrophages [39], assessing apoptosis [40], the characterization of differences in the Raman signature between normal and cancerous cells [41–43], or the analysis and identification of microbial cultures [44, 45].

For example, Chan and co-workers [42] demonstrated better than 98% sensitivity in their ability to separate live hematopoietic cells from immortalized, neoplastic cell lines utilizing laser tweezers confocal Raman micro-spectroscopy and principal component analysis. They found that differences between normal and cancer cells were quantified mostly based on differences in the local cellular concentration and the relative ratios of DNA and protein vibrations. Immortalized cell lines will inherently show less variation in individual cell spectra than pathological samples obtained from patients which led the same group to further demonstrate that they could identify individual leukemic T and B cells in blood samples obtained from juvenile leukemia patients [46]. Similarly, other groups have recently shown that they are able to distinguish cells obtained from various tumors (brain, pancreas, liver, etc.) from normal cells opening up the potential to develop Raman spectroscopy into a universal analysis tool without the need for expensive reagents with limited shelf life [43, 47, 48]. A remaining challenge to analyzing cells by spontaneous Raman spectroscopy is the relatively long signal integration time required to obtain useful Raman spectra from individual cells, which can range from seconds to minutes. Broadband coherent Raman scattering utilizing either CARS or SRS might eventually replace this mechanism if suitable and cost-effective means can be found to integrate short-pulsed lasers with rapid flow analysis. The holy grail of this technique is, of course, the hunt for and the identification of rare cells, such as circulating tumor cells or circulating stem cells.

On the subcellular scale, intracellular compartments, vesicles, organelles and macromolecular

complexes are typically the target of Raman spectroscopy. In particular, the analysis of lipid-cell interactions in living cells, the main problem underlying most lipid disorders in humans, has become one of the leading objectives of intracellular Raman spectroscopy. This is mostly due to the fact that cells that are exposed to an abundance of lipids, such as free fatty acids, diglycerides, and triglycerides often develop lipid inclusions, or lipid droplets, in their cytoplasm as part of their response mechanism to fight lipotoxicity. Because of the sample concentration requirement of spontaneous Raman spectroscopy, lipid droplets represent ideal targets for Raman-based analysis because they typically accumulate lipids in concentrated form as spherical droplets ranging from few tens of nanometers up to several microns in diameter. These studies are further aided by the fact that Raman spectroscopy can easily distinguish between different lipids or lipid states, such as saturated and unsaturated fatty acids, triglycerides, oxidized lipids, etc. (see Figs. 3 and 4). At the current time we simply have no other means to perform similar analyses of individual lipid droplets and their prolonged development, in living cells. The analysis of such complex lipid mixtures, however, requires additional advanced chemometricstechniques, such as hierarchical cluster analysis or least discriminant analysis (LDA) in order to determine the precise lipid composition of these structures

Coherent Raman imaging techniques are particularly interesting on these length scales, because they enable the rapid and repetitive imaging of cells as they develop lipid inclusions, while also allowing for the analysis of the lipid composition (Figs. 4 and 5 and references [49, 50]). This enables the acquisition of dynamic data on the second and sub-second time scale as shown in the example of Nan et al. who first demonstrated dynamic imaging of intracellular organelle transport without exogenous dyes in steroidogenic mouse adrenal cortical cells [51].

Another example demonstrating the utility of Raman-based imaging is the tracking of the infection pathways of Hepatitis C, which are very difficult, if not impossible to study by other means. The Hepatitis C Virus (HCV) is believed to spread by hiding inside triglyceride-rich lipoprotein particles, such as very low-density lipoproteins (VLDL). While some studies have been conducted using fluorescent markers, such exogenous labels may perturb and alter the behavior of lipid droplets and their associated proteins. Nan et al. for example, were able to correlate lipid droplet density with HCV density in human hepatoma cells using a combination of fluorescence and CARS imaging [52]. More recently, Rinia and coworkers used multiplex CARS microscopy to obtain quantitative images of similar lipid droplets and measure the composition and distribution of different species of lipids within a single droplet. Their work demonstrated that cells that took up lipids from their surrounding environment formed small droplets that later fused with the larger droplets that already resided in the cytoplasm [50]. This paper, as well as other similar work, has opened up an entirely new way of studying lipid interactions with cells. Coherent Raman microscopy is currently the only technique capable of rapidly and quantitatively imaging lipid dynamics in living cells without altering them. A challenge, however, remains the

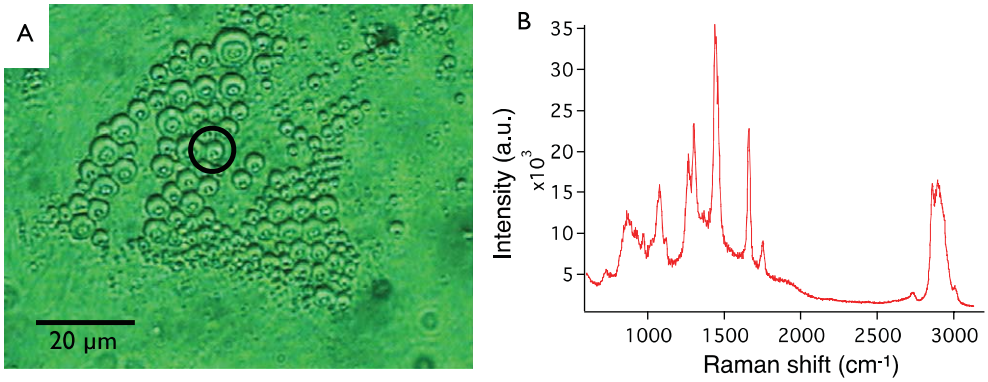

Fig. 3. A) Differential interference contrast image of a human mesenchymal stem cell differentiatedinto an adipocyte as evident by the large number of lipid droplets. B) Raman spectrum of the lipid droplet highlighted in A). The spectrum indicates the presence of mostly unsaturated lipids in the form of di- and triglycerides.

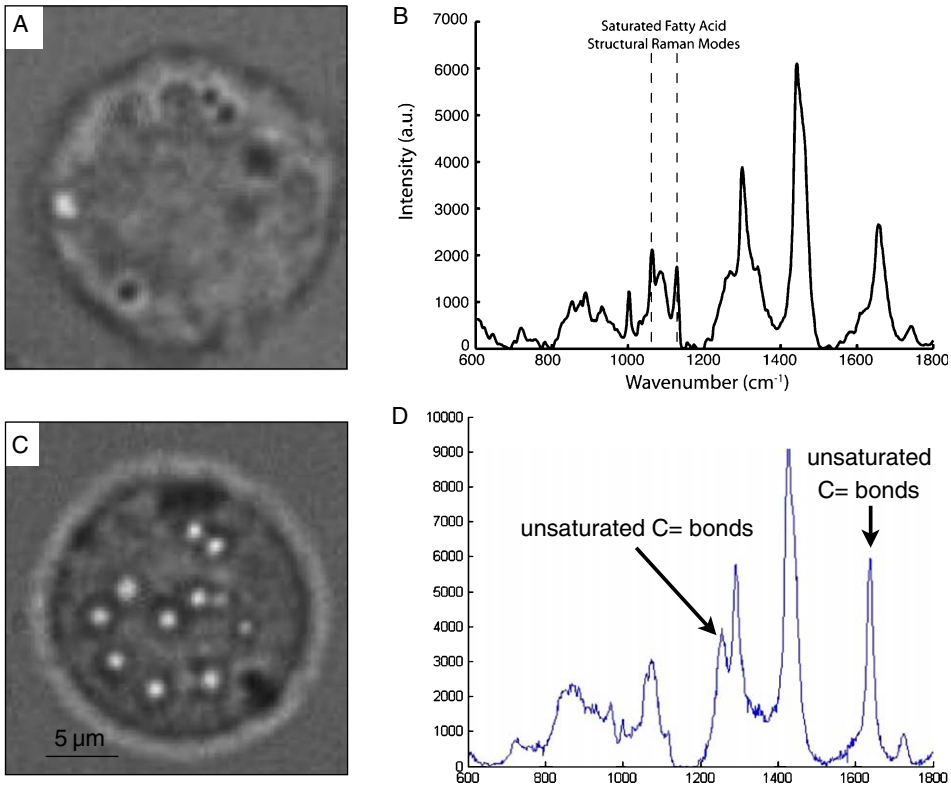

Fig. 4. Human THP-1 monocytes treated with lipoprotein lipolysis products. A) CARS image of a monocyte at 2845 cm^{-1} exhibiting increased saturated fatty acids in lipid inclusions as indicated by the associated Raman spectrum (B). C) CARS image of a monocyte with lipid droplets consisting of mostly unsaturated fatty acids as indicated by the associated Raman spectrum (D).

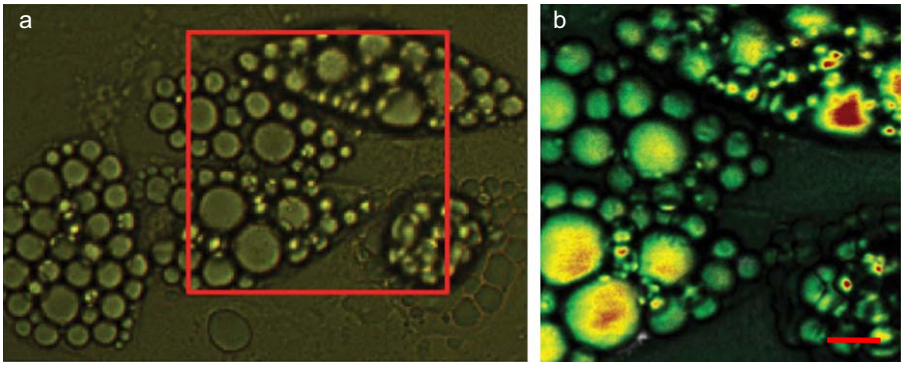

Fig. 5. a) Differential interference contrast image of a human mesenchymal stem cells differentiatedinto adipocytes containing many large lipid droplets. b) CARS image of the area highlighted in a by scanning the sample at the 2845 cm^{-1} aliphatic lipid vibration. Scale bar: 5 µm.

sensitivity limit of these techniques, which requires sample concentrations in the high micromolar to millimolar range. Overcoming this limitation requires additional tricks, such as e.g. the application of doubly-resonant CARS microscopy, where an abundant Raman resonance can be utilized to amplify the signal of a weaker resonance [53–55].

Lately, embryonic stem cells and their derivatives have become a popular target or Raman-based studies [56]. Pluripotent cells carry a number of unique

characteristics that show up in their Raman-spectroscopic signature, i.e. as increased cytoplasmic levels of glycogen and a distorted intranuclear protein-DNA ratio, that can be used to characterize these cells, determine their differentiation state, and, ideally isolate them from the larger population of yet uncommitted cells [57–59]. This is particularly important if these cells are to be purified for therapeutic applications, because e.g. antibody or aptamer-based biochemical methods will activate and/or contaminate these cells. Raman spectroscopy requires no reagents and has no detrimental effects on cell health, which is why Raman-based flow sorting would be highly desirable. This, however, will likely again require the use of multiplex coherent Raman technique in order to meet the time scales required to efficiently sort large populations of cells.

4. Raman scattering of tissues

4.1. Cancer diagnosis

Raman scattering has been used extensively to assess disease states in tissues. As shown in the preceding sections, Raman spectroscopy has been used to non-invasively discriminate cancerous from noncancerous cells in solution. This same ability can be extended to tissues, where Raman spectroscopy can provide a compelling complement to traditional dissection and H&E (hematoxylin and eosin) staining. H&E staining provides primarily structural information while Raman spectroscopy and Raman imaging provide a detailed picture of the underlying chemical changes that accompany carcinogenesis.

Several groups have pursued this direction, with promising results. In an early paper on the subject, Mizuno et al. showed spectral changes associated with glioma carcinogenesis, with quantitative spectral differences being observed between grade II and grade III disease [60]. Nijssen et al. demonstrated the ability of Raman mapping, where Raman spectra are acquired at hundreds of points on a section of tissue to form a low-resolution hyperspectral image, to discriminate basal cell carcinoma from surrounding normal tissue [61]. These results are shown in Fig. 6, adapted from [61].

Majumder et al. examined Raman spectroscopy and two other optical biopsy techniques, namely autofluorescence and diffuse reflectance, comparing their ability to discriminate between normal breast tissue, fibroadenoma, ductal carcinoma *in situ*, and invasive ductal carninoma [62]. Their results show that although autofluorescence and diffuse reflectance have the ability to classify samples, especially when used jointly, Raman spectroscopy alone gives superior classification accuracy, with a Hand and Till measure (an extension of the traditional sensitivity and specificity metrics to multiclass classification) of 0.99 (compared to an ideal of 1.0). The examination of more than one class of disease in this work is an important aspect to note. Raman spectroscopy has shown considerable power in discriminating between not just normal and diseased tissue, but between different types and stages of disease. For example, Chowdary et al. demonstrated that

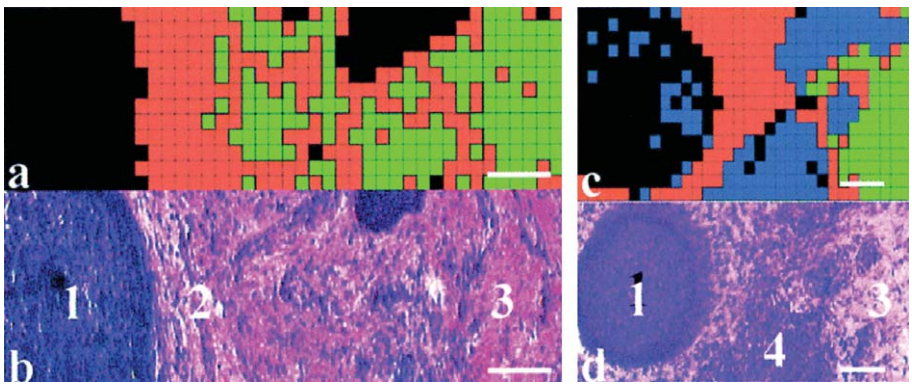

Fig. 6. Comparison of pseudo-color Raman maps (a, c) with images (b, d) of H&E-stained adjacent sections. Black = BCC; red and green = dermis; blue = dense chronic inflammatory infiltrate. 1 = BCC; 2 = collagen-poor dermis; 3 = collagen-rich dermis; 4 = chronic inflammatory infiltrate. Scale bar: 100 m. Reprinted by permission from Macmillan Publishers Ltd: Journal of Investigative Dermatology, Ref. 61, 2002.

Raman spectroscopy can distinguish between benign and malignant lesions within breast tissue [63].

One factor that is common to all of the above studies is a reliance on multivariate statistical methods for extracting meaningful information from the information rich Raman spectrum. Although Raman spectroscopy is typically hailed for its ability to provide an information-rich spectrum, the same chemical specificity which allows it to classify samples with high accuracy can also make real-world application of the technique challenging. Typical multivariate models are generated by measuring hundreds of spectra from hundreds of samples, and then submitting this information to a machine learning algorithm that searches for correlations between spectra that have been defined as belonging to a specific class. A new, unrelated set of spectra (the so-called validation set) is then submitted to the trained algorithm and the samples are classified based on the features and correlations deduced from the training set. Extension of these multivariate models to spectra taken on different instruments, by different users, or on different patients, is a problem known as calibration transfer. The challenges of calibration transfer is one reason why Raman spectroscopy has not seen more widespread adoption in clinical settings. The sensitivity of Raman spectroscopy means that a spectrum reports on all variations between one patient and another, most of which are unrelated to disease state and generally serve only to confound the multivariate model. The group of Mahadevan-Jansen has extensively examined the spectral changes between samples that are all labeled histologically normal [64, 65]. In these works, the authors have shown that there are strong spectral differences in the cervix related to both menopausal status and position within the menstrual cycle. In addition, there are differences between the Raman spectra from cervices that have had a previous history of disease versus those that might be thought of as "true normals".

Several groups have explored various methodologies to reduce this potentially confounding biological variability. One technique explored by Chen et al. involves measuring cells scraped from the colon lining *ex vivo*, as single cells stripped of the surrounding tissue components often show much lower biological variability [43]. Smith and Berger demonstrated a technique using polarization to select only those photons which have explored the most superficial layers of tissue. Since many tumors reside in the surface layers of tissue, this could reduce variability arising from spectral components in the deeper layers of tissue [66]. Matousek and Stone have explored various novel instrument geometries that have the potential to reduce confounding artifacts. In one paper, they have shown the ability of a Raman system to detect a calcified inclusion within a thick layer of tissue, with potential applications to breast cancer diagnosis [67]. Matousek has also pioneered spatially offset Raman spectroscopy (SORS), where excitation photons are launched from an optical fiber into a tissue at one location and collected through a second fiber at a small distance from the source fiber. The distance between the source and collection fiber determines the volume explored by the measurement. Through appropriate choice of source-collection distances, one can make depth-resolved measurements of the bulk tissue, potentially removing biological variability by suppressing signal from pathologically uninteresting layers [68].

One intriguing result of Raman spectroscopy's exquisite chemical sensitivity is the prospect of using Raman spectroscopy to detect the cancer field effect. First described in 1953 [69], the cancer field effect describes both a situation in which a cancerous cell exerts an influence on its surrounding environment, as well as the idea that carcinogenesis is a symptom of a broader, tissue-level disorder. The cancer field effect has been compellingly explored optically by Backman et al. [70] through the use of elastic light scattering. However, two studies have pointed to the potential of Raman spectroscopy to detect the changes in tissue chemistry of normal tissue due to the presence of cancerous cells in the vicinity [65, 71]. Most compellingly, Lieber et al. have recently demonstrated that spectral differences can be found between normal organotypic raft cultures that have been cultured either in the presence or absence of cancer cells. It is important to note that the cancer cells in these studies were not in physical contact with the raft cultures, but rather simply shared culture media, providing a conduit for cell-cell signaling.

The preceding studies all utilized spontaneous Raman spectroscopy to perform cancer diagnosis. But it is important to note that some work has been done using coherent variants of Raman spectroscopy as well. Ji-Xin Cheng and co-authors recently published a compelling article utilizing the previously described CARS imaging technique to perform intravital flow cytometry - where cytometry is performed on cells flowing through a single capillary *in vivo* – using CARS imaging of a lipid resonance as a contrast mechanism to

detect circulating tumor cells [72]. Demonstrating the feasibility of detecting CTCs using CARS imaging has obviously important implications for cancer detection and treatment.

These important studies point to Raman spectroscopy's power to diagnosis cancer based on the chemical changes undergone during the process of carcinogenesis. Although challenges remain in using appropriate multivariate techniques to extract meaningful variations within the complicated Raman spectra from the uninteresting variations occurring due to normal biological processes, the prospects for *in vivo* diagnosis of cancer through Raman biopsy are promising.

4.2. Raman spectroscopy of vasculature

A particular application of Raman spectroscopy is to detection of vulnerable plaques and other coronary diseases. Several early papers by Michael Feld and co-authors [73, 74] established the ability of Raman spectroscopy to detect spectral differences between normal coronary tissues and various plaques, including calcified, fibrous, and atheromatous plaques based on samples studied *ex vivo*. These signals were correlated with results from biochemical assays, with the excellent agreement pointing to Raman spectroscopy's power as a quantitative assay technique. These results were replicated *in vivo* by Buschman et al. in an animal model utilizing specially designed fiber probes allowing high quality Raman signals to be detected through long segments of optical fiber [75]. More recently, Motz et al. measured *in vivo* spectra of arterial plaques during peripheral vascular surgery. Spectra taken were analyzed by fitting acquired spectra to a model composed of 9 chemical constituents. The results were then compared with traditional morphological assessment during routine confirmational histology. The results indicated the ability of Raman spectroscopy to diagnose *in vivo* several arterial pathologies including intimal fibroplasia, atheromatous plaques, calcified plaques, ruptured plaques, and thrombotic plaques [76]. Further *in vivo* results have been presented utilizing both fingerprint and high-wavenumber spectra of a human artery through the use of a specially designed fiber probe [77].

Meanwhile, CARS has very recently been demonstrated in an *ex vivo* human artery [78]. CARS, in conjunction with two-photon fluorescence and second harmonic generation, provide an image with some chemical sensitivity. False color images were demonstrated where two-photon fluorescence reports mainly on elastin, second harmonic generation reports on collagen, while CARS signals are mainly due to lipid content.

The ability of Raman spectroscopy to diagnose vulnerable plaques has been the subject of much promising study for over 20 years. However, only recently has it become feasible to create fiber probes both small and flexible enough to enter a human artery while still retaining the ability to acquire high quality Raman signals with integration times on the scale of 1 second or less.

4.3. Other applications of Raman spectroscopy to tissue

Raman spectroscopy has found applications beyond those major topics discussed above. Due to its chemical sensitivity it can be used in many applications where morphology alone is not enough to determine disease type. Gniadecka et al. have shown that cutaneous tophi and calcinosis, two nodule forming pathologies with similar clinical presentations, can be diagnosed quite easily through the presence of monosodium urate bands or hydroxyapatite bands within the Raman spectrum [79].

In a recent study regarding wound healing, Crane et al. demonstrated that Raman spectra of severe wounds sustained by service members in Operations Iraqi Freedom and Enduring Freedom have predictive ability with regards to whether the wounds will heal normally or have impaired healing [80]. This is principally a function of the collagen content of the wounds, with impaired healing wounds lacking adequate collagen deposition. They also show the evolution of the Raman spectra of tissue removed from a normal healing wound at the first and last debridement, shown in Fig. 8 (adapted from [80]).

The ability to noninvasively monitor wound health is undoubtedly a pressing unmet need in hospital settings.

Another application is the determination of chemical profiles of particular analytes within tissue. For example, Caspers et al. used confocal Raman microspectroscopy to determine the hydration level of skin versus depth [81], reporting on several analytes comprising the so-called natural moisturizing factor. Concentration profiles such as these could be used to

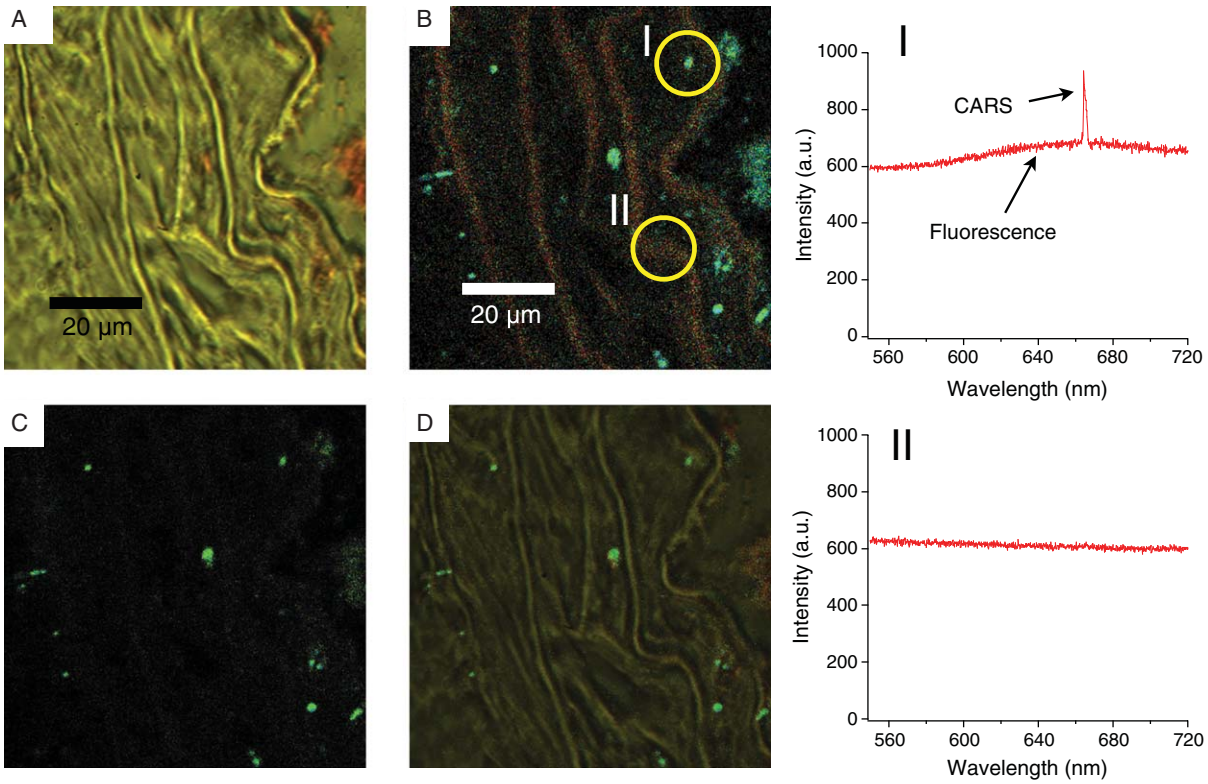

Fig. 7. Coherent Anti-Stokes Raman Scattering (CARS) microscopy of mouse aorta thin section stained with H&E stain and oil-red O. A) White light transmitted light micrograph of the stained tissue section. Oil-red O stained lipids appear red. B) Time-correlated CARS image of the same tissue section. Areas with a photon arrival time within the instrument response function of the system appear green, while delayed photons due to fluorescence appear red. Spectra obtained from the highlighted areas are shown to the right. The sharp peak at 665 nm in (I) represents a CARS peak from the 2845 cm^{-1} Raman mode of aliphatic C–H bonds representative of lipids. The spectrum obtained in area (II) exhibits no CARS contributions and only broad fluorescence background. This is additional proof that the green areas shown in (B) are entirely due to CARS signals from lipids. C) Time-gated CARS micrograph of the same tissue section. Time-gating for photons arriving within the fast instrument response selects on CARS signals and rejects any fluorescence contributions. D) Overlay of the transmitted light image (A) with the time-gated CARS image (C).

monitor, for example, drug delivery from a topically applied solution.

Coherent techniques have a role to play in this area as well. In 2005, Evans et al. demonstrated video-rate CARS imaging of lipids *in vivo* [82]. As discussed in that article, the technique opens up possibilities for real time imaging of drug diffusion and metabolism as well as other pathologically relevant applications.

5. Pathogen analysis by Raman spectroscopy

Raman spectroscopy has been used in several applications for pathogen analysis and typing. The ability of Raman spectroscopy to measure bacteria either on culture medium, *in situ*, or to measure single bacteria in solution has the potential to greatly reduce the need for labor and time-intensive culturing of bacteria on selective media to determine the identity of a particular pathogen.

Andrew Berger and co-authors have done extensive research on oral bacteria, showing the ability of Raman spectroscopy to quantify different bacterial species in polymicrobial mixtures [83] and in intact biofilms [19]. The ability to separate different bacterial species in a native, mixed environment demonstrates the power of Raman spectroscopy to rapidly characterize pathogens without waiting for culture.

Rösch et al. further this technique by extending it to Raman spectra of single bacteria, such as might be

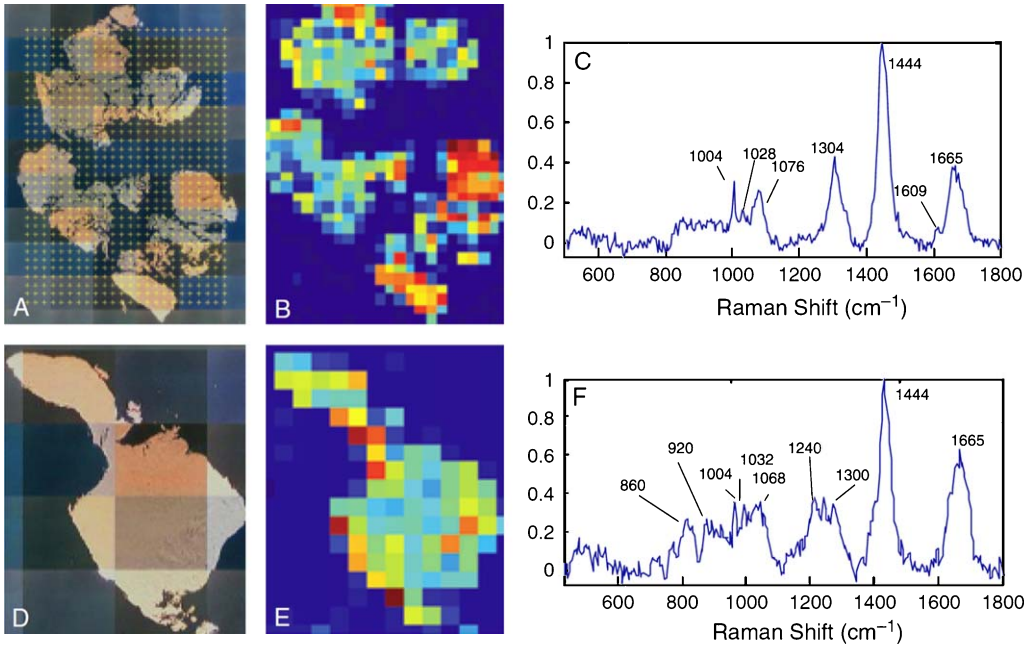

Fig. 8. Visible images of tissue sections for a normal healing wound at first (A) and last (D) debridements. Corresponding score images (B and E) and components (C and F) are shown. Each pixel in the score image is approximately 100 × 100 μm. Adapted with permission from Ref. 80.

found on the air filter in a clean room environment [21]. Through the use of support vector machines, a multivariate machine learning algorithm, the authors report recognition rates for different bacterial species of over 90%. The authors also record high resolution Raman maps of the single bacteria and bacterial spores. The hyperspectral maps, shown in Fig. 9 (adapted from [21]), clearly show spatial variation of band intensities across the bacterium, information which could be utilized in studies of bacterial growth or metabolism.

Intriguingly, the authors also claim ∼80–90% classification accuracy for recognizing different strains of the same bacterial species. This important result was replicated on a different system by Maquelin et al. for different strains of *Acinetobacterbaumannii,* a major cause of hospital infections [84]. Using isolates from five known hospital outbreaks of the bacterium, Raman spectra were recorded alongside genetic analyses. By simply smearing the bacteria onto a CaF_2 slide and measuring the spectrum, then submitting the measured spectra to a simple principal components/hierarchical clustering analysis, the bacteria could be typed by strain with only one misclassification out of 25 samples.

Neugebauer et al. explored the spatial variation of Raman spectra within bacteria using tip-enhanced Raman spectroscopy (TERS) to provide exquisite spatial localization [85]. TERS is closely related to the above-described surface-enhanced Raman scattering, where a metal tip provides the plamon resonance and field enhancement. By scanning a silver-coated silicon tip with a nominal apex diameter of 50 nm, TERS spectra were acquired across a bacterium with spatial resolutions limited only by the tip diameter. This provides the possibility to examine dynamics and processes that occur directly on the surface of the bacterial wall, and important site of attack for many antibiotics, and an important point of antibiotic defense for drug resistant bacteria. This was further explored in a later paper where time-dependent fluctuations of TERS peaks were observing a single point on a bacterial cell wall [86].

CARS has also been used for imaging of bacterial spores. In Fig. 10, the image of spores takes advantage of a strong Raman resonance at 1013 cm^{-1} due to calcium dipicolinate in dormant spores.

Several groups have investigated the ability of Raman spectroscopy to elucidate mechanisms of action of antibiotics. As described in a paper by López-Diez et al. the rate at which new antibiotics are being developed is declining while the rate at which many important human pathogens are acquiring multi-drug

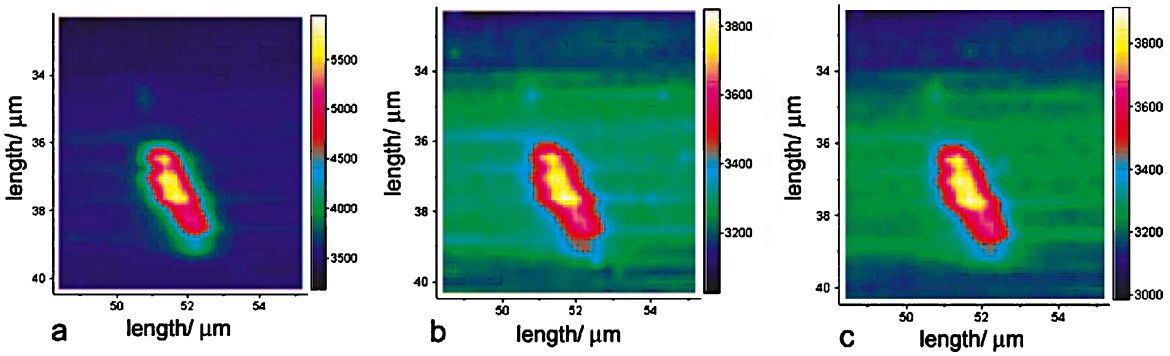

Fig. 9. Raman maps of a single bacterium (B. sphaericus DSM 28) for three different wavenumber regions: a, 2851 to 2964 cm^{-1}; b, 1604 to 1671 cm^{-1}; and c, 1410 to 1455 cm^{-1}. Reproduced with permission from American Society for Microbiology, Ref. 21.

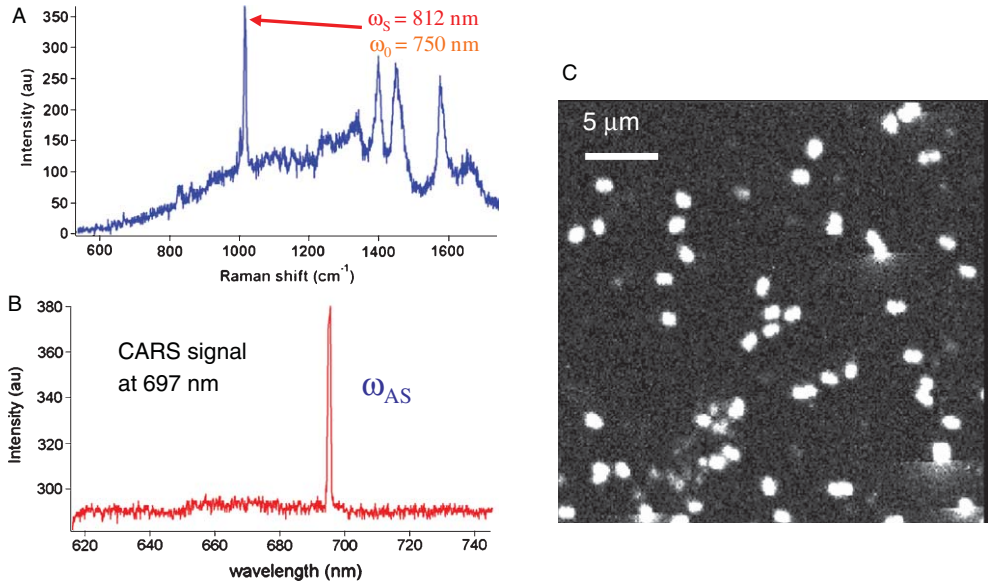

Fig. 10. A) Raman spectrum of bacterial spores of Bacillus subtilis. The strong peak at 1013 cm^{-1} is due to calcium dipicolinate in the dormant spores. B) The beams of two picosecond lasers were tuned to the calcium dipicolinate vibration resulting in strong coherent anti-Stokes Raman scattering at 697 nm. C) CARS image the bacterial spores adhered to a glass surface when imaged at the 697 nm resonance.

resistance is increasing [87]. Therefore, there is a pressing need for tools to enable rapid drug development and characterization, as well as a need for tools within a hospital environment to determine if a particular drug is an effective antibiotic agent for a particular patient or outbreak. In the López-Diez paper, the authors use UV resonance Raman spectroscopy, which preferentially reports on bands associated with nucleic acids and amino acids, to assess chemical changes upon treatment of *Pseudomonas aeruginosa* with amikacin. The results show that not only do the spectra report on known rRNA damage and associated protein synthesis inhibition, but they also can quantitatively separate inhibitory versus subinhibitory concentrations of the drug. Moritz et al. have also reported on Raman spectroscopic markers of drug action in a study examining the effect of cefazolin on individual, living *E. coli* bacteria [88]. Through monitoring the bacteria at different time points along their growth curve, spectral changes are noted that correlate strongly to the concentration of drug applied. This has led the authors to hypothesize that one mechanism of action of cefazolin may

be related to non-enzymatic glycosylation of the bacterial DNA, leading to an abnormal arrest of bacterial replication by causing the bacteria to enter stationary phase.

Besides the obvious industrial utility of helping to assess toxicity of candidate drugs and helping to elucidate mechanisms of drug action, the ability to noninvasively characterize the response of individual bacteria to antibiotics may provide valuable insight to a clinician in helping to determine an appropriate course of treatment for a particular patient, enabling more targeted and efficacious therapies.

6. Conclusions and outlook

Raman scattering in pathology is still a relatively new science. Its potential has been demonstrated so far for a range of applications, including label-free analysis of cells, tissues, and detection of certain pathogens.

After initially relatively slow adoption, an increasing number of studies have incorporated Raman scattering for characterization of cancer cells, microbiological cultures, and to determine the interactions of drugs with cells, especially in cases where fluorescent probes are not suitable (small molecules) or are limiting due to e.g. photo-bleaching. For rapid live cell imaging different modalities of coherent Raman scattering are now widely utilized and are even available from commercial sources. These methods are now also beginning to find their way into the latest areas of biomedical research, such as regenerative medicine, where biochemical methods can often do more harm than good.

Another area of intense research is the development of portable, fiber-based Raman devices that enable the use of Raman spectroscopy for *in-vivo* endoscopies, in clinical settings, or in the field, with potential for real-time optical biopsy in pathology. While this is a very exciting direction, problems such as intrinsic fluorescence signal generated in the tissue by the excitation laser, and background Raman and fluorescence signals produced by most fibers when the excitation light passes through them will have to properly be addressed.

A particularly interesting prospect for Raman spectroscopy is its ability to utilize minor changes in molecular structure to create unique optical markers, similar to fluorescent labels, but significantly less intrusive and at the same time robust to photodecomposition. A relatively easy to implement change in molecular structure is for example the isotope-exchange of deuterium for hydrogen. In deuterated molecules, the high wavenumber active C-H bond in the $2850\,cm^{-1}$ range is shifted to significantly lower wavenumbers of $\sim 2200\,cm^{-1}$ for C-D vibrations. Furthermore, this signal occurs in a spectral region that for most biomolecules is entirely flat and featureless. Thus, this marker peak now enables one to isolate and track deuterated molecules and distinguish them from the bulk of non-modified molecules. This is particularly useful for small molecules, such as lipids or sugars, the function and processing of which would otherwise be significantly limited by the need to attach large fluorescent molecules to them.

Another potential prospect is the advent of super-resolving methods in fluorescence microscopies, i.e., optical tools that make imaging beyond the diffraction limit possible. The most prominent current implementation of these far-field super-resolving methods are stimulated emission depletion (STED), single molecule localization techniques, and structured illumination microscopy. STED could possibly be implemented in coherent Raman imaging modalities, whereas structured illumination is compatible with spontaneous Raman spectroscopy. First proposals to develop these modalities have been published but it remains to be seen how these will be implemented practically in the future.

In addition, combination of Raman scattering with other methods including immunohistochemistry, flow cytometry, laser capture micro-dissection, and quantitative imaging is very attractive for enhanced sensitivity and specificity of detection. In many cases, Raman scattering can be utilized alongside traditional sample collection and analysis techniques to provide an additional dimension of information.

In conclusion, Raman scattering is a powerful technique, which can monitor subtle biochemical changes within cells and tissues without the need for invasive labels. Despite challenges involving low signal strengths and competing backgrounds, Raman spectroscopy has already been applied to several problems of clinical interest for pathologists. However, closer collaborations between pathologists and spectroscopists is needed to identify and approach unmet clinical needs in pathology to bring Raman scattering out of laboratory environments and into widespread clinical practice.

References

[1] S. Wachsmann-Hogiu, T. Weeks and T. Huser, Chemical analysis *in vivo* and *in vitro* by Raman spectroscopy–from single cells to humans, *Current Opinion in Biotechnology* **20** (2009), 63–73.

[2] F. Knorr, Z.J. Smith and S. Wachsmann-Hogiu, Development of a time-gated system for Raman spectroscopy of biological samples, *Optics express* **18** (2010), 20049–20058.

[3] M.D. Duncan, J. Reintjes and T.J. Manuccia, Scanning coherent anti-stokes Raman microscope. *Optics Letters* **7** (1982), 350–352.

[4] A. Zumbusch, G.R. Holtom and X.S. Xie, Three-dimensional vibrational imaging by coherent anti-Stokes Raman scattering. *Physical Review Letters* (1999), pp. 4142–4145.

[5] B.G. Saar, C.W. Freudiger, J. Reichman, C.M. Stanley, G.R. Holtom, et al., Video-rate molecular imaging *in vivo* with stimulated Raman scattering. *Science* **330** (2010), 1368–1370.

[6] M.C. Wang, W. Min, C.W. Freudiger, G. Ruvkun and X.S. Xie, RNAi screening for fat regulatory genes with SRS microscopy, *Nature Methods* **8** (2011), 135–138.

[7] C.V. Pagba, S.M. Lane, H. Cho and S. Wachsmann-Hogiu, Direct detection of aptamer-thrombin binding via surface-enhanced Raman spectroscopy, *Journal of Biomedical Optics* **15** (2010), 047006.

[8] M. Sha, S. Penn, G. Freeman and W. Doering, Detection of human viral RNA via a combined fluorescence and SERS molecular beacon assay, *NanoBioTechnology* **3** (2007), 23–30.

[9] H. Cho, B.R. Baker, S. Wachsmann-Hogiu, C.V. Pagba, T.A. Laurence, et al., Aptamer-Based SERRS Sensor for Thrombin detection, Nano Letters, 2008, 4386–4390.

[10] R.J. Stokes, E. McBride, C.G. Wilson, J.M. Girkin, W.E. Smith, et al., Surface-enhanced Raman scattering spectroscopy as a sensitive and selective technique for the detection of folic acid in water and human serum, *Applied Spectroscopy* **62** (2008), 371–376.

[11] M. Lin, L. He, J. Awika, L. Yang, D.R. Ledoux, et al., Detection of melamine in gluten, chicken feed, and processed foods using surface enhanced Raman spectroscopy and HPLC, *Journal of Food Science* **73** (2008), T129–T134.

[12] M. Green, F.M. Liu, L. Cohen, P. Kollensperger and T. Cass, SERS platforms for high density DNA arrays, *Faraday Discussions* **132** (2006), 269–280.

[13] A. Pal, N.R. Isola, J.P. Alarie, D.L. Stokes and T. Vo-Dinh, Synthesis and characterization of SERS gene probe for BRCA-1 (breast cancer), *Faraday Discussions* **132** (2006), 293–301.

[14] C.A. Lieber and A. Mahadevan-Jansen, Automated method for subtraction of fluorescence from biological Raman spectra, *Applied spectroscopy* **57** (2003), 1363–1367.

[15] B.D. Beier and A.J. Berger, Method for automated background subtraction from Raman spectra containing known contaminants, *The Analyst* **134** (2009), 1198–1202.

[16] A.C. De Luca, M. Mazilu, A. Riches, C.S. Herrington and K. Dholakia, Online fluorescence suppression in modulated Raman spectroscopy, *Analytical Chemistry* **82** (2010), 738–745.

[17] A.P. Shreve, N.J. Cherepy and R.A. Mathies, Effective rejection of fluorescence interference in Raman-spectroscopy using a shifted excitation difference technique, *Applied Spectroscopy* **46** (1992), 707–711.

[18] J.W. Chan, D.S. Taylor, S.M. Lane, T. Zwerdling, J. Tuscano, et al., Nondestructive identification of individual leukemia cells by laser trapping Raman spectroscopy, *Analytical Chemistry* **80** (2008), 2180–2187.

[19] B.D. Beier, R.G. Quivey and A.J. Berger, Identification of different bacterial species in biofilms using confocal Raman microscopy, *Journal of Biomedical Optics* **15** (2010), 066001.

[20] M. Gniadecka, P.A. Philipsen, S. Sigurdsson, S. Wessel, O.F. Nielsen, et al., Melanoma diagnosis by Raman spectroscopy and neural networks: Structure alterations in proteins and lipids in intact cancer tissue, *Journal of Investigative Dermatology* **122** (2004), 443–449.

[21] P. Rosch, M. Harz, M. Schmitt, K.D. Peschke, O. Ronneberger, et al., Chemotaxonomic identification of single bacteria by micro-Raman spectroscopy: Application to clean-room-relevant biological contaminations, *Applied and Environmental microbiology* **71** (2005), 1626–1637.

[22] C. Matthaus, T. Chernenko, J.A. Newmark, C.M. Warner and M. Diem, Label-free detection of mitochondrial distribution in cells by nonresonant Raman microspectroscopy, *Biophysical Journal* **93** (2007), 668–673.

[23] C. Krafft, M.A. Diderhoshan, P. Recknagel, M. Miljkovic, M. Bauer, et al., Crisp and soft multivariate methods visualize individual cell nuclei in Raman images of liver tissue sections, *Vibrational Spectroscopy* **55** (2011), 90–100.

[24] G.J. Puppels, F.F.M. Demul, C. Otto, J. Greve, M. Robert-nicoud, et al., Studying single living cells and chromosomes by confocal Raman microspectroscopy, *Nature* **V347** (1990), 301–303.

[25] J.W. Chan, S. Fore, S. Wachsmann-Hogiu and T. Huser, Raman spectroscopy and microscopy of individual cells and cellular components, *Laser and Photonics Reviews* **2** (2008), 325–349.

[26] G.J. Puppels, W. Colier, J.H.F. Olminkhof, C. Otto, F.F.M. Demul, et al., Description and performance of a highly sensitive confocal Raman microspectrometer, *Journal of Raman Spectroscopy* **V22** (1991), 217–225.

[27] G.J. Puppels, J.H.F. Olminkhof, G.M.J. Segersnolten, C. Otto, F.F.M. Demul, et al., Laser irradiation and Raman spectroscopy of single living cells and chromosomes - sample degradation occurs with 514.5 nm but not with 660 nm laser light, *Experimental Cell Research* **V195** (1991), 361–367.

[28] C.G. Xie, M.A. Dinno and Y.Q. Li, Near-infrared Raman spectroscopy of single optically trapped biological cells, *Optics Letters* **27** (2002), 249–251.

[29] C.G. Xie and Y.Q. Li, Confocal micro-Raman spectroscopy of single biological cells using optical trapping and shifted excitation difference techniques, *Journal of Applied Physics* **93** (2003), 2982–2986.

[30] J.W. Chan, A.P. Esposito, C.E. Talley, C.W. Hollars, S.M. Lane, et al., Reagentless identification of single bacterial spores in aqueous solution by confocal laser tweezers Raman spectroscopy, *Analytical Chemistry* **76** (2004), 599–603.

[31] K. Ramser, K. Logg, M. Goksor, J. Enger, M. Kall, et al., Resonance Raman spectroscopy of optically trapped functional erythrocytes, *Journal of Biomedical Optics* **9** (2004), 593–600.

[32] C.J. de Grauw, C. Otto and J. Greve, Line-scan Raman microspectrometry for biological applications, *Applied Spectroscopy* **51** (1997), 1607–1612.
[33] G.J. Puppels, M. Grond and J. Greve, Direct imaging Raman microscope based on tunable wavelength excitation and narrow-band emission detection, *Applied Spectroscopy* **V47** (1993), 1256–1267.
[34] J.X. Cheng, Y.K. Jia, G. Zheng and X.S. Xie, Laser-scanning coherent anti-Stokes Raman scattering microscopy and applications to cell biology, *Biophysical Journal* **83** (2002), 502–509.
[35] C.W. Freudiger, W. Min, B.G. Saar, S. Lu, G.R. Holtom, et al., Label-free biomedical imaging with high sensitivity by stimulated Raman scattering microscopy, *Science* **322** (2008), 1857–1861.
[36] G.J. Puppels, C. Otto and J. Greve, Confocal Raman microspectroscopy in biology - applications and future developments, *Trac-Trends in Analytical Chemistry* **V10** (1991), 249–253.
[37] G.J. Puppels, H.S.P. Garritsen, G.M.J. Segersnolten, F.F.M. Demul and J. Greve, Raman microspectroscopic approach to the study of human granulocytes, *Biophysical Journal* **V60** (1991), 1046–1056.
[38] M.D. Mannie, T.J. McConnell, C.G. Xie and Y.Q. Li, Activation-dependent phases of T cells distinguished by use of optical tweezers and near infrared Raman spectroscopy, *Journal of Immunological Methods* **297** (2005), 53–60.
[39] H.J. van Manen, Y.M. Kraan, D. Roos and C. Otto, Single-cell Raman and fluorescence microscopy reveal the association of lipid bodies with phagosomes in leukocytes, *Proceedings of the National Academy of Sciences of the United States of America* **102** (2005), 10159–10164.
[40] N. Uzunbajakava, A. Lenferink, Y. Kraan, E. Volokhina, G. Vrensen, et al., Nonresonant confocal Raman imaging of DNA and protein distribution in apoptotic cells, *Biophysical Journal* **84** (2003), 3968–3981.
[41] Y. Yazdi, N. Ramanujam, R. Lotan, M.F. Mitchell, W. Hittelman, et al., Resonance Raman spectroscopy at 257 nm excitation of normal and malignant cultured breast and cervical cells, *Applied Spectroscopy* **53** (1999), 82–85.
[42] J.W. Chan, D.S. Taylor, T. Zwerdling, S.M. Lane, K. Ihara, et al., Micro-Raman spectroscopy detects individual neoplastic and normal hematopoietic cells, *Biophysical Journal* **90** (2006), 648–656.
[43] K. Chen, Y.J. Qin, F. Zheng, M.H. Sun and D.R. Shi, Diagnosis of colorectal cancer using Raman spectroscopy of laser-trapped single living epithelial cells, *Optics Letters* **31** (2006), 2015–2017.
[44] K. Maquelin, L.P. Choo-Smith, T. van Vreeswijk, H.P. Endtz, B. Smith, et al., Raman spectroscopic method for identification of clinically relevant microorganisms growing on solid culture medium, *Analytical Chemistry* **V72** (2000), 12–19.
[45] L.P. Choo-Smith, K. Maquelin, T. van Vreeswijk, H.A. Bruining, G.J. Puppels, et al., Investigating microbial (micro)colony heterogeneity by vibrational spectroscopy, *Applied and Environmental Microbiology* **V67** (2001), 1461–1469.
[46] J.W. Chan, D.S. Taylor, S. Lane, T. Zwerdling, J. Tuscano, et al., Non-destructive identification of individual Leukemia cells by laser tweezers Raman spectroscopy, *Anal Chem* **80** (2008), 2180–2187.
[47] M.A. Short, H. Lui, D. McLean, H.S. Zeng, A. Alajlan, et al., Changes in nuclei and peritumoral collagen within nodular basal cell carcinomas via confocal micro-Raman spectroscopy, *Journal of Biomedical Optics* **11** (2006), 034004.
[48] A. Taleb, J. Diamond, J.J. McGarvey, J.R. Beattie, C. Toland, et al., Raman microscopy for the chemometric analysis of tumor cells. *Journal of Physical Chemistry B* **110** (2006), 19625–19631.
[49] K.N.J. Burger, H.A. Rinia, M. Bonn, and M. Muller, Label-free cellular imaging of lipid composition of individual lipid droplets using multiplex CARS microscopy. *Chemistry and Physics of Lipids* **154** (2008), S5–S5.
[50] H.A. Rinia, K.N.J. Burger, M. Bonn and M. Müller, Quantitative label-free imaging of lipid composition and packing of individual cellular lipid droplets using multiplex CARS microscopy, *Biophysical Journal* **95** (2008), 4908–4914.
[51] X. Nan, E.O. Potma and X.S. Xie, Nonperturbative chemical imaging of organelle transport in living cells with coherent anti-stokes Raman scattering microscopy, *Biophysical Journal* **91** (2006), 728–735.
[52] X.L. Nan, A.M. Tonary, A. Stolow, X.S. Xie and J.P. Pezacki, Intracellular imaging of HCV RNA and cellular lipids by using simultaneous two-photon fluorescence and coherent anti-stokes Raman scattering microscopies, *Chembiochem* **7** (2006), 1895–1897.
[53] T. Weeks, S. Wachsmann-Hogiu and T. Huser, Raman microscopy based on Doubly-Resonant Four-Wave Mixing (DR-FWM), *Optics Express* **17** (2009), 17044–17051.
[54] T. Weeks, I. Schie, S. Wachsmann-Hogiu and T. Huser, Signal generation and Raman-resonant imaging by non-degenerate four-wave mixing under tight focusing conditions, *J Biophoton* **3** (2010), 169–175.
[55] T. Weeks, I.W. Schie, L.J. den Hartigh, J.C. Rutledge and T. Huser, Lipid-cell interactions in human monocytes investigated by doubly-resonant coherent anti-Stokes Raman scattering microscopy, *J Biomed Opt* **16** (2011), 021117-021111 - 021117–021115.
[56] I. Notingher, I. Bisson, A.E. Bishop, W.L. Randle, J.M.P. Polak, et al., *In Situ* spectral monitoring of mRNA translation in embryonic stem cells during differentiation *in vitro*, *Anal Chem* **76** (2004), 3185–3193.
[57] J. Chan, D. Lieu, T. Huser, R. Li, Label-free spectroscopic separation of human embryonic stem cells (hESCs) and their cardiac derivatives using Raman spectroscopy. *Anal Chem* **81** (2009), 1324–1331.
[58] H.G. Schulze, S.O. Konorov, N.J. Caron, J.M. Piret, M.W. Blades, et al., Assessing differentiation status of human embryonic stem cells noninvasively using Raman microspectroscopy, *Anal Chem* **82** (2010), 5020–5027.
[59] S.O. Konorov, H.G. Schulze, J.M. Piret, R.F.B. Turner, M.W. Blades, Evidence of marked glycogen variations in the characteristic Raman signatures of human embryonic stem cells. *J Raman Spectrosc* (2011), DOI 10.1002/jrs.2829: in print.
[60] A. Mizuno, H. Kitajima, K. Kawauchi, S. Muraishi and Y. Ozaki, Near-Infrared Fourier-Transform Raman-Spectroscopic Study of Human Brain-Tissues and Tumors, *Journal of Raman Spectroscopy* **25** (1994), 25–29.

[61] A. Nijssen, T.C.B. Schut, F. Heule, P.J. Caspers, D.P. Hayes, et al., Discriminating basal cell carcinoma from its surrounding tissue by Raman spectroscopy, *Journal of Investigative Dermatology* **119** (2002), 64–69.

[62] S.K. Majumder, M.D. Keller, F.I. Boulos, M.C. Kelley and A. Mahadevan-Jansen, Comparison of autofluorescence, diffuse reflectance, and Raman spectroscopy for breast tissue discrimination, *Journal of Biomedical Optics* **13** (2008).

[63] M.V.P. Chowdary, K.K. Kumar, J. Kurien, S. Mathew and C.M. Krishna, Discrimination of normal, benign, and malignant breast tissues by Raman spectroscopy, *Biopolymers* **83** (2006), 556–569 .

[64] E.M. Kanter, S. Majumder, G.J. Kanter, E.M. Woeste, A. Mahadevan-Jansen, Effect of hormonal variation on Raman spectra for cervical disease detection. *American Journal of Obstetrics and Gynecology* **200** (2009), 512e1–512e5.

[65] M.D. Keller, E.M. Kanter, C.A. Lieber, S.K. Majumder, J. Hutchings, et al., Detecting temporal and spatial effects of epithelial cancers with Raman spectroscopy, *Disease Markers* **25** (2008), 323–337.

[66] Z.J. Smith and A.J. Berger, Surface-sensitive polarized Raman spectroscopy of biological tissue, *Optics Letters* **30** (2005), 1363–1365.

[67] P. Matousek and N. Stone, Prospects for the diagnosis of breast cancer by noninvasive probing of calcifications using transmission Raman spectroscopy, *Journal of Biomedical Optics* **12** (2007), 024008.

[68] N. Stone, R. Baker, K. Rogers, A.W. Parker and P. Matousek, Subsurface probing of calcifications with spatially offset Raman spectroscopy (SORS): Future possibilities for the diagnosis of breast cancer, *Analyst* **132** (2007), 899–905.

[69] D.P. Slaughter, H.W. Southwick and W. Smejkal, Field cancerization in oral stratified squamous epithelium - clinical implications of multicentric origin, *Cancer* **6** (1953), 963–968.

[70] H. Subramanian, P. Pradhan, Y. Liu, I.R. Capoglu, X. Li, et al., Optical methodology for detecting histologically unapparent nanoscale consequences of genetic alterations in biological cells, *Proceedings of the National Academy of Sciences of the United States of America* **105** (2008), 20118–20123.

[71] C.A. Lieber, H.E. Nethercott and M.H. Kabeer, Cancer field effects in normal tissues revealed by Raman spectroscopy, *Biomedical optics express* **1** (2010), 975–982.

[72] T.T. Le, T.B. Huff and J.X. Cheng, Coherent anti-Stokes Raman scattering imaging of lipids in cancer metastasis. *Bmc Cancer* **9** (2009), 42.

[73] J.J. Baraga, M.S. Feld and R.P. Rava, *In situ* optical histochemistry of human artery using near-infrared fourier-transform Raman-Spectroscopy, *Proceedings of the National Academy of Sciences of the United States of America* **89** (1992), 3473–3477.

[74] J.F. Brennan, T.J. Romer, R.S. Lees, A.M. Tercyak, J.R. Kramer, et al., Determination of human coronary artery composition by Raman spectroscopy, *Circulation* **96** (1997), 99–105.

[75] H.P. Buschman, E.T. Marple, M.L. Wach, B. Bennett, T.C.B. Schut, et al., *In vivo* determination of the molecular composition of artery wall by intravascular Raman spectroscopy, *Analytical Chemistry* **72** (2000), 3771–3775.

[76] J.T. Motz, M. Fitzmaurice, A. Miller, S.J. Gandhi, A.S. Haka, et al., *In vivo* Raman spectral pathology of human atherosclerosis and vulnerable plaque, *Journal of Biomedical Optics* **11** (2006), 021003.

[77] A.H. Chau, J.T. Motz, J.A. Gardecki, S. Waxman, B.E. Bouma, et al., Fingerprint and high-wavenumber Raman spectroscopy in a human-swine coronary xenograft *in vivo*. *Journal of Biomedical Optics* **13** (2008), 040501.

[78] L.B. Mostaco-Guidolin, M.G. Sowa, A. Ridsdale, A.F. Pegoraro, M.S. Smith, et al., Differentiating atherosclerotic plaque burden in arterial tissues using femtosecond CARS-based multimodal nonlinear optical imaging, *Biomedical optics express* **1** (2010), 59–73.

[79] M. Gniadecka, H.C. Wulf, C.K. Johansson, S. Ullman, P. Halberg, et al., Cutaneous tophi and calcinosis diagnosed *in vivo* by Raman spectroscopy, *British Journal of Dermatology* **145** (2001), 672–674.

[80] N.J. Crane, T.S. Brown, K.N. Evans, J.S. Hawksworth, S. Hussey, et al., Monitoring the healing of combat wounds using Raman spectroscopic mapping, *Wound Repair and Regeneration* **18** (2010), 409–416.

[81] P.J. Caspers, G.W. Lucassen, E.A. Carter, H.A. Bruining and G.J. Puppels, *In vivo* confocal Raman microspectroscopy of the skin: Noninvasive determination of molecular concentration profiles, *Journal of Investigative Dermatology* **116** (2001), 434–442.

[82] C.L. Evans, E.O. Potma, M. Puoris'haag, D. Cote, C.P. Lin, et al., Chemical imaging of tissue *in vivo* with video-rate coherent anti-stokes Raman scattering microscopy, *Proceedings of the National Academy of Sciences of the United States of America* **102** (2005), 16807–16812.

[83] Q. Zhu, R.G. Quivey and A.J. Berger, Measurement of bacterial concentration fractions in polymicrobial mixtures by Raman microspectroscopy, *Journal of Biomedical Optics* **9** (2004), 1182–1186.

[84] K. Maquelin, L. Dijkshoorn, T.J. van der Reijden and G.J. Puppels, Rapid epidemiological analysis of Acinetobacter strains by Raman spectroscopy, *Journal of Microbiological Methods* **64** (2006), 126–131.

[85] U. Neugebauer, P. Rosch, M. Schmitt, J. Popp, C. Julien, et al., On the way to nanometer-sized information of the bacterial surface by tip-enhanced Raman spectroscopy, *Chemphyschem: A European Journal of Chemical Physics and Physical Chemistry* **7** (2006), 1428–1430.

[86] U. Neugebauer, U. Schmid, K. Baumann, W. Ziebuhr, S. Kozitskaya, et al., Towards a detailed understanding of bacterial metabolism–spectroscopic characterization of Staphylococcus epidermidis, *Chemphyschem: A European Journal of Chemical Physics and Physical Chemistry* **8** (2007), 124–137.

[87] E.C. Lopez-Diez, C.L. Winder, L. Ashton, F. Currie and R. Goodacre, Monitoring the mode of action of antibiotics using Raman spectroscopy: Investigating subinhibitory effects of amikacin on Pseudomonas aeruginosa, *Analytical Chemistry* **77** (2005), 2901–2906.

[88] T.J. Moritz, D.S. Taylor, C.R. Polage, D.M. Krol, S.M. Lane, et al., Effect of cefazolin treatment on the nonresonant Raman signatures of the metabolic state of individual Escherichia coli cells, *Analytical Chemistry* **82** (2010), 2703–2710.